OPEN ACCESS Freely available online

PLoS one

Intra-Cluster Percolation of Calcium Signals

Guillermo Solovey*¤, Silvina Ponce Dawson

Departamento de Física, Facultad de Ciencias Exactas y Naturales - Universidad de Buenos Aires, Buenos Aires, Argentina

Abstract

Calcium signals are involved in a large variety of physiological processes. Their versatility relies on the diversity of spatio-temporal behaviors that the calcium concentration can display. Calcium entry through inositol 1,4,5-trisphosphate (IP_3) receptors (IP_3R's) is a key component that participates in both local signals such as "puffs" and in global waves. IP_3R's are usually organized in clusters on the membrane of the endoplasmic reticulum and their spatial distribution has important effects on the resulting signal. Recent high resolution observations [1] of Ca^{2+} puffs offer a window to study intra-cluster organization. The experiments give the distribution of the number of IP_3R's that open during each puff without much processing. Here we present a simple model with which we interpret the experimental distribution in terms of two stochastic processes: IP_3 binding and unbinding and Ca^{2+}-mediated inter-channel coupling. Depending on the parameters of the system, the distribution may be dominated by one or the other process. The transition between both extreme cases is similar to a percolation process. We show how, from an analysis of the experimental distribution, information can be obtained on the relative weight of the two processes. The largest distance over which Ca^{2+}-mediated coupling acts and the density of IP_3-bound IP_3R's of the cluster can also be estimated. The approach allows us to infer properties of the interactions among the channels of the cluster from statistical information on their emergent collective behavior.

Citation: Solovey G, Dawson SP (2010) Intra-Cluster Percolation of Calcium Signals. PLoS ONE 5(2): e8997. doi:10.1371/journal.pone.0008997

Editor: Giuseppe Chirico, University of Milano-Bicocca, Italy

Received October 28, 2009; **Accepted** January 11, 2010; **Published** February 18, 2010

Funding: This work was supported by Proyecto de Investigación Científica y Tecnológica (PICT) 17-21001 granted by Agencia Nacional de Promocion Cientifica y Tecnologica (ANPCyT, http://www.agencia.gov.ar/), and by Proyecto de Investigación Plurianual (PIP) 112-200801-01612 granted by Consejo Nacional de Investigaciones Científicas y Técnicas (CONICET) UBA (http://www.uba.ar/secyt/subsidios/index.php), Santa Fe Institute (http://www.santafe.edu/). The funders had no role in study design, data collection and analysis, decision to publish, or preparation of the manuscript.

Competing Interests: The authors have declared that no competing interests exist.

* E-mail: gsolovey@df.uba.ar

¤ Current address: Laboratory of Mathematical Physics, Rockefeller University, New York, New York, United States of America

Introduction

The calcium (Ca^{2+}) ion is a universal second messenger that is involved in a large number of physiological processes [2]. To this end, cells regulate cytosolic Ca^{2+} concentration ($[Ca^{2+}]$) very precisely. At basal conditions free cytosolic $[Ca^{2+}]$ is very low ($\sim 100nM$). $[Ca^{2+}]$ is several orders of magnitude higher in the extracellular medium and in internal reservoirs, such as the endoplasmic reticulum. Different signals can induce the opening of specific Ca^{2+} channels located on the plasma membrane or on the membrane of the internal reservoirs leading to local increments of the cytosolic $[Ca^{2+}]$ of various durations. This $[Ca^{2+}]$ change evokes different end responses depending upon the spatio-temporal distribution of $[Ca^{2+}]$. Thus, it is of interest to measure the latter and how different factors shape it.

One of the Ca^{2+} channels involved in intracellular Ca^{2+} signals is the inositol 1,4,5-trisphosphate (IP_3) receptor (IP_3R) which is expressed in many cell types and is located at the surface of intracellular membranes such as the endoplasmic reticulum (ER), the sarcoplasmic reticulum (SR) and the nucleus. The IP_3R is biphasically regulated by Ca^{2+}, with a bell-shaped open probability as a function of $[Ca^{2+}]$. Kinetic models of the IP_3R take this dual effect into account by assuming that the receptor has at least one activating and one inhibitory site such that Ca^{2+} binding to the first one induces channel opening (provided that IP_3 is also bound to the receptor) and Ca^{2+} binding to the second one induces channel closing [3–5]. Given that the affinity for Ca^{2+} of the activating site is larger than that of the inhibitory site, a local increase of cytosolic Ca^{2+} in the vicinity of an IP_3R with IP_3 bound induces channel opening first. This leads to a phenomenon called Ca^{2+}-induced Ca^{2+}-release (CICR) because the Ca^{2+} ions released by one channel can in turn trigger the opening of other nearby channels with IP_3 bound. Ca^{2+} channels are not uniformly distributed in the cell. IP_3R's, in particular, are usually organized in clusters on the membrane of the ER that are separated by a few microns [6]. These clusters have been estimated to be $400nm \times 400nm$ in size in oocytes [7,8]. The simulations of [7] showed that previous observations could be reproduced assuming that between 25 and 35 IP_3R's opened simultaneously during puffs. A similar estimate was obtained in [8] using a mean-field model that assumed that all channels opened and closed simultaneously. Simulations that include a stochastic description of the individual channel openings and closings, however, show that at most half of the channels with IP_3 bound are simultaneously open during a puff [8]. This implies that even in clusters with 50 IP_3R's with IP_3 bound, the maximum number of simultaneously open channels is around 20. These results are consistent with observations of Ca^{2+} signals in the human neuroblastoma SY5Y cell line in which puffs of up to 20 simultaneously open channels were observed [1]. Measurements performed using patches of the outer nuclear envelope of the DT40 cell line give smaller numbers of IP_3R's in each patch [9]. The non-uniform spatial organization of the IP_3R's together with the channel coupling induced by CICR gives rise to a large variety

of intracellular Ca^{2+} signals that go from very localized ones to waves that propagate throughout the cell [10].

The hierarchy of intracellular Ca^{2+} signals that includes Ca^{2+} "blips" (Ca^{2+} release through a single IP_3R), "puffs" (Ca^{2+} release through several IP_3R's in a cluster) and waves that propagate globally across cells by successive cycles of CICR has been observed using fluorescence microscopy and Ca^{2+} sensitive dyes [10–13]. The *Xenopus laevis* oocyte has been frequently used for this purpose because of its relatively large size and because the only Ca^{2+} channels that are present on the surface of the ER are IP_3R's. Fluorescent images of these signals obtained with confocal microscopy do not resolve the inner-cluster structure. Therefore, different modeling strategies have been presented in order to determine the properties of the dynamics and spatial organization of IP_3R's within clusters that are compatible with these experimental observations [7,8,14,15]. In particular, in [8,16] we made the very simple assumption that the number of IP_3R's that open during the first puff that occurs at a site is given by the number of IP_3R's with IP_3 bound. The underlying assumption was that the Ca^{2+} released by the first open channel would induce the opening of all the other IP_3R's of the cluster with IP_3 bound. Therefore, if all the clusters had approximately the same number of IP_3R's and all IP_3R's were equally sensitive to IP_3, the distribution of the number of channels that opened during a puff could be approximated by a binomial or Poisson distribution [8], provided that the probability that the channels become open were the same immediately before the occurrence of each puff. This last condition would not be satisfied in a non-stationary situation, *e.g.* if the concentrations of the agonists right before the release event differed significantly from puff to puff. It would not hold, in particular, for data containing sequences of puffs that are coupled through CICR or to puffs in which the inhibitory effect of the Ca^{2+} released in a previous event was noticeable, as described in [16]. In oocytes, the latter is only relevant for very long records containing many puffs at a site, which is usually not the case in most experiments. Calcium induced calcium release is also affected by buffers that can trap Ca^{2+} ions as they diffuse. This not only reduces the $[Ca^{2+}]$ but also alters the rate of Ca^{2+} transport [17]. The distances that separate IP_3R's within a cluster are very small (10–20nm) [9]. Thus, only large concentrations of very fast buffers could affect Ca^{2+}-mediated inter-channel coupling in cases with many active channels [18,19]. The assumption that all the channels with IP_3 bound participate of the first puff of their site is the simplest way of approaching the complex problem of Ca^{2+}-mediated inter-channel communication. Yet, it is applicable as long as the distance between IP_3-bound channels is not too large. In the present paper we drop this assumption and analyze how Ca^{2+}-mediated inter-channel coupling affects the distribution of puff sizes. Our approach provides a simple tool to study some of the effects of buffers on the intra-cluster dynamics.

The quantal properties of Ca^{2+} release during puffs have recently been revealed in [1] using total internal reflection fluorescence (TIRF) microscopy in intact mammalian cells of the human neuroblastoma SY5Y cell line. The proximity of IP_3R's to the plasma membrane in this cell type allowed the use of TIRF microscopy in which fluorescence can be elicited in a very small (attoliter) volume. This, together with the use of a fast CCD camera, permitted a much better temporal resolution than the one achieved with confocal microscopy. In this way, abrupt step-wise transitions between fluorescence levels were observed during the falling phase of puffs. Furthermore, many puffs could be elicited at each release site due to the use of a membrane-permeable form of IP_3 [20]. The authors then inferred that the step-wise transitions between fluorescence levels occurred in multiples of a basic unit that they identified with the amplitude contribution of each channel at the site [1]. Using this relationship they could readily obtain the distribution of the number of channels that open during a puff. Given that there is a large variability among cluster sites, they analyzed the subset of events that occur in clusters with a similar number of IP_3R's. The authors did not find any sign of an inhibiting effect of the Ca^{2+} released in their records. In spite of that and even constraining the data set as mentioned before, they found that a Poisson distribution failed to reproduce the observed histogram of event sizes particularly in the region of small events (*i.e.*, puffs with very few open channels). They could approximately describe the distribution with a model that assumes a weak cooperativity among channels. Inter-channel cooperativity is mediated by the Ca^{2+} released through an open IP_3R that subsequently diffuses to a neighboring channel. Thus, the distance between channels is a key factor that regulates the cooperativity strength [21]. The approach of [1], however, does not take space into account.

In the present paper we introduce a simple model that takes into account both the stochasticity due to IP_3 binding and the distance-dependent Ca^{2+}-mediated cooperativity. It can reproduce the event size distribution reported in [1] for events involving any number of open channels. The distribution obtained with our model approaches a binomial or Poisson distribution as the cooperativity strength increases so that the opening of one IP_3R induces the opening of all other IP_3R's with IP_3 bound. This transition from Ca^{2+}-dominated to IP_3-binding dominated stochasticity is similar to a percolation transition. It also occurs if the number of IP_3R's with IP_3 bound increases. Therefore, the transition can be reflected on the distribution of the number of IP_3R's that open at a given release site.

Percolation in connection with Ca^{2+} signals has been invoked to explain the transition from abortive to propagating waves in cells [22–24]. Our paper is the first to identify two limiting regimes of the intra-cluster dynamics that underlies puffs and to characterize the change between them as a percolation transition. Furthermore, we show how information on the transition between both regimes (the IP_3-binding and the Ca^{2+} dominated behaviors) can be extracted from the distribution of the number of IP_3R's that open during a puff. Knowledge on this transition can, in turn, yield information on the largest distance over which Ca^{2+}-mediated cooperativity acts and on the mean density of IP_3-bound IP_3R's of the clusters. In this way, we can estimate biophysical parameters that affect the intra-cluster dynamics from statistical information on the emergent collective behavior of the channels of the cluster.

The aim of the simple model that we introduce in this paper is to characterize the basic mechanisms that shape the distribution of the number of channels that open during puffs. In particular, we identify the competition between two stochastic processes as the main determinant of the form of the distribution. Therefore, an analysis of this form may give information on the relative weight of the two competing processes. The model does not include a detailed description of the dynamics that takes place during or between events. For some time most models of intracellular Ca^{2+} dynamics were deterministic (see *e.g.* [25]). The observation of local signals such as puffs led to the development of several models that included a stochastic description of Ca^{2+} release [14,15,26,27] or of the spatial location of the IP_3R's [28]. It is currently clear that stochastic effects are not only relevant for local release events but are a fundamental aspect of the Ca^{2+} dynamics for the full range of observed signals, including waves [29–32]. More information on stochastic models of Ca^{2+} signals can be found in a recent focus issue on the subject [33]. Simulations of

these stochastic dynamic models could be used to probe the main findings of the present paper.

Results

The Model

We introduce here a simple model to describe the distribution of puff sizes that occur at sites with similar numbers of IP_3R's. The model is simple in the sense that it does not include a detailed description of the dynamics of the individual channel openings and closings or of IP_3 or Ca^{2+} binding and unbinding. However, it does include the stochasticity associated to IP_3 binding and channel coupling via CICR. Given the estimates of [8], the model assumes that clusters occupy a fixed size region (more specifically, a circle of radius, R) and that N IP_3R's are randomly distributed over the cluster region with uniform probability. Each IP_3R of the cluster has a probability p of having IP_3 bound. N_p is the random variable that represents the number of available IP_3R's (*i.e.*, of IP_3R's with IP_3 bound) of the cluster before a puff starts. The distribution of this variable is a binomial of parameters N and p, that can be approximated by a Poisson distribution of parameter $\lambda=pN$ for N large and p small enough (for example, with $N=20$ and $p=0.05$ the absolute difference between both cumulative distributions is lower than 0.01 for each N_p). The model considers that if an IP_3R with IP_3 bound becomes open and Ca^{2+} starts to flow through its pore all other IP_3R's with IP_3 bound that are within a distance, r_{inf}, of the open IP_3R will also become open. These newly opened IP_3R's in turn trigger the opening of new IP_3R's with IP_3 bound that are within the distance, r_{inf}, from an open one. This scheme triggers a cascade of openings that stops when there are no more available IP_3R's within the radius of influence (*i.e.*, the distance r_{inf}) of any open IP_3R. This cascade determines the number, n, of channels that open during a puff. We call $P_A(N_p)$ the probability that there are N_p available IP_3R's (with IP_3 bound) in a cluster and $P_o(n/N_p)$ the conditional probability that n channels open during an event given that there are N_p with IP_3 bound in the cluster. Given that we are interested in the distribution of event sizes, we only consider the situations for which $1\leq n\leq N_p$. Therefore, we renormalize the probabilities so that $\sum_{N_p=1}^{N} P_A(N_p)=1$ and $\sum_{n=1}^{N_p} P_o(n/N_p)=1$. In this way, $P_A(N_p)$ is a binomial or a Poisson distribution divided by one minus the probability that there are not IP_3R's with IP_3 bound in the cluster. Using these renormalized versions of $P_A(N_p)$ and $P_o(n/N_p)$, the probability, P_n, of having a puff with n open channels is given by:

$$P_n=\sum_{N_p\geq n}^{N} P_o(n/N_p)P_A(N_p), \qquad n\geq 1. \tag{1}$$

$P_A(N_p)$ is approximated by a Poisson distribution of parameter $\lambda=pN$ when $N\to\infty$. P_n can be readily compared with distributions obtained from experimental observations as the one displayed in Fig. 4D of [1].

Factors That Shape the Distribution of Event Sizes

The two stochastic components of the model are evident in the expression of P_n. $P_A(N_p)$ reflects the stochasticity of IP_3 binding and $P_o(n/N_p)$ the one due to inter-channel coupling via CICR. The relative weight of both factors on the resulting P_n depends on the relationship between two typical lengthscales of the problem: the radius of influence, r_{inf} (the maximum distance between channels at which CICR still works) and the mean distance between channels with IP_3 bound, D, which is a random variable that can be computed in terms of R and the number of IP_3R's with IP_3 bound, N_p, as:

$$D(N_p)=\frac{R}{2}\sqrt{\frac{\pi}{N_p}}, \qquad N_p>1. \tag{2}$$

D can take values between 0 and $R\sqrt{\pi}/2$. Closely related to D is the density of available IP_3R's which is given by:

$$\rho_A\equiv\frac{N_p}{\pi R^2}. \tag{3}$$

ρ_A and D are related by: $4D^2=1/\rho_A$.

The relationship between D and r_{inf} determines the relative weight of both stochastic components on P_n. In particular, if r_{inf}/D is very large, the opening of any channel of the cluster will eventually lead to the opening of all other available channels. If such a situation holds for most events, then $P_o(n/N_p)\approx\delta_{nN_p}$ and P_n will mainly be determined by the stochastic component due to IP_3 binding, *i.e.*, $P_n\approx P_A(n)$. If, for most events, r_{inf}/D is very small, then most of P_n will be concentrated near $n=1$, regardless of how many available IP_3R's there are in each realization. We will refer to both extreme behaviors as IP_3 or Ca^{2+} limited. Depending on the parameters of the model (R, r_{inf}, N, and p), one or the other situation is favored. However, in many situations one or the other behavior is favored depending on the value of N_p, *i.e.*, on the realization. In those cases, the dominant stochastic component of P_n depends on the value of n.

We first illustrate how the distribution, P_n, varies with the number of IP_3R's of the cluster, N, while all other parameters are fixed. As N increases, the most likely values that N_p can take on also increase. This means that it is more probable to have more available IP_3R's at any given instance. On the other hand, since the spatial dimensions of the cluster are unchanged (R is fixed) the mean distance between available IP_3R's, D, is more likely to be smaller (see Eq. 2). Given that the typical distance for CICR to occur, r_{inf}, is also fixed, it is more probable that r_{inf}/D be larger. Therefore, P_n approaches P_A as N is increased. This is illustrated in Fig. 1 where we have plotted the distributions P_n (solid circles) and $P_A(N_p)$ (bars) obtained with 1000 realizations of our model using $p=5/18$, $R=250nm$, $r_{inf}=230nm$ and three values of N. In A, $N=10$, the number of available channels is small for most realizations (its mean value is $m=pN=2.8$) so that P_n is dominated by inter-channel Ca^{2+}-coupling and concentrated around small values of n. In C, $N=50$, the number of available channels is large for most realizations (its mean value is $m=pN=13.9$) so that D is typically smaller than r_{inf} ($D(13.9)=59.43nm$). In this case, P_n is dominated by the IP_3-binding stochasticity and almost indistinguishable from the distribution of available channels, P_A. The example of Fig. 1 B corresponds to a situation in between these two extreme cases with $N=20$. We can observe how, as the number of available channels is more likely to be larger, P_n approaches P_A. We also observe that for $N=10$ and $N=20$, P_n and P_A differ mainly in the region of small values of n. This occurs because it is difficult for one open channel to induce the opening of another one if the mean inter-channel distance is large. Thus, if N_p is small it is very rare that all available channels become open. In this way, the relative frequency of small events becomes larger than the fraction of instances with a small number of available channels.

A transition from Ca^{2+}-dominated to IP_3-binding dominated stochasticity also occurs as r_{inf} is increased, while all other parameters are fixed. In this case, P_A remains unchanged and so

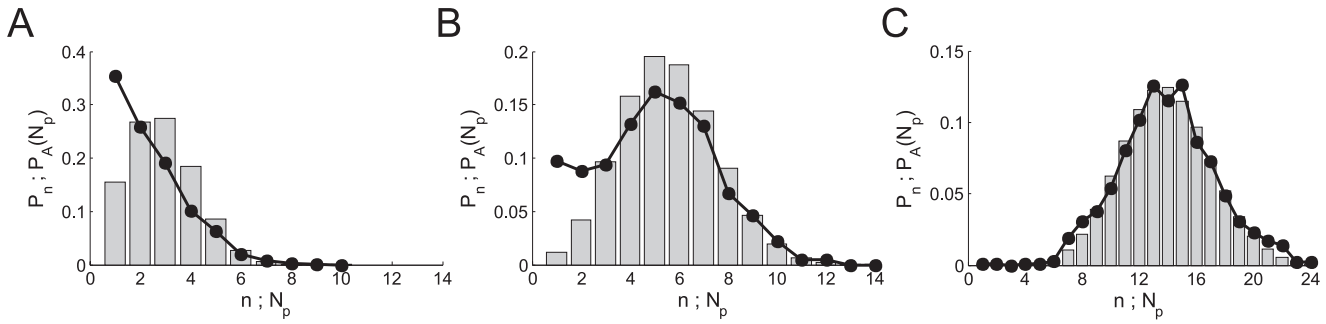

Figure 1. Distribution of puff sizes: transition between Ca^{2+}-dominated to IP_3-binding dominated stochasticity. Solid circles: distribution of puff sizes, P_n, obtained with our model for $p=5/18$, $R=250nm$, $r_{inf}=230nm$ and three values of N: $N=10$ (A), $N=20$ (B) and $N=50$ (C). Histograms (in grey): corresponding distributions of available channels, $P_A(N_p)$ for the same parameter values. All distributions were computed from 1000 realizations for each set of parameters.
doi:10.1371/journal.pone.0008997.g001

does the mean distance between available IP_3R's, D. By changing r_{inf} it is possible to go from a situation in which r_{inf}/D is small for most events and P_n is Ca^{2+}-limited to a situation in which r_{inf}/D is large and P_n is IP_3-binding limited. This is illustrated in Fig. 2 where we have plotted the distribution of event sizes that we obtain with our model for three different values of r_{inf}. For $r_{inf}=150nm$, the distribution is Ca^{2+}-coupling limited and is concentrated around $n=1$. As r_{inf} is increased, the relative frequency of events with small n decreases. For $r_{inf}=500nm$, the distribution is IP_3-binding limited. In this example, P_A is well approximated by a Poisson distribution of parameter $\lambda=5$ (data not shown). The situation in between these extreme cases corresponds to $r_{inf}=250nm$ and is able to reproduce reasonably well the experimental distribution of Fig. 4D of [1] (superimposed with bars in Fig. 2).

In the Ca^{2+} limited behavior the number of open channels, n, is small for most events, regardless of the value of N_p. This implies $n<N_p$ for almost all events. In the IP_3-binding limited behavior all available IP_3R's become open ($n=N_p$ in most cases). Therefore, in

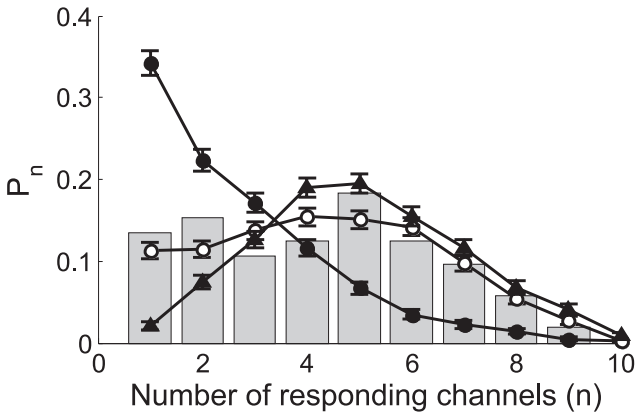

Figure 2. Distribution of puff sizes: change of behavior with the radius of influence and comparison with observations. We show the probabiliy, P_n, of having a puff with n open channels obtained with our model for $N=18$, $p=5/18$, $R=250nm$ and $r_{inf}=150nm$ (solid circles), $r_{inf}=250nm$ (open circles) and $r_{inf}=500nm$ (triangles). Each curve corresponds to 500 realizations of the model. We observe a transition from a Ca^{2+}-dominated to a IP_3-binding dominated stochasticity distribution as r_{inf} increases. Superimposed with bars: experimental data taken from Fig. 4D of [1].
doi:10.1371/journal.pone.0008997.g002

order to analyze the transition between the Ca^{2+}-dominated to IP_3-binding dominated stochasticity, we study how often events occur for which all available IP_3R's become open. This happens trivially for events with $N_p=1$. Here we are interested in situations with $N_p>1$. To this end, we compute numerically the probability that all available IP_3R's, N_p, become open, $P(n=N_p/N_p)$, which is a function of N_p and of only one independent parameter, the dimensionless radius of influence, r_{inf}/R, (see Methods). We plot in Fig. 3 A $P(n=N_p/N_p)$ as a function of r_{inf}/R, for $N_p=10$ (circles), $N_p=30$ (squares) and $N_p=100$ (triangles). As expected, $P(n=N_p/N_p)$ is an increasing function of N_p for each value of r_{inf}/R. We also observe that $P(n=N_p/Np)$ is an increasing (sigmoidal-like) function of r_{inf}/R that goes from 0 (*i.e.* $n<N_p$ in almost all cases, which corresponds to Ca^{2+}-dominated stochasticity) to 1 (*i.e.* $n=N_p$ in almost all cases, which corresponds to IP_3-binding dominated stochasticity) and that such transition occurs over a smaller interval of r_{inf}/R values the larger N_p is.

We can think of the Ca^{2+}-limited and the IP_3-binding limited situations as two phases and the transition between them as a phase transition in the limit of very large N_p. This percolation-like transition occurs at a well defined value of r_{inf}/R in this limit. For finite values of N_p we introduce two quantities, $r_{inf}^{(1)}(N_p)$ and $r_{inf}^{(2)}(N_p)$, that determine the type of regime that we can expect (Ca^{2+}-limited if $r_{inf}<r_{inf}^{(1)}$ or IP_3-binding limited if $r_{inf}>r_{inf}^{(2)}$) for each value of N_p (see Methods). The arrows in Fig. 3 A indicate the values of $r_{inf}^{(1)}/R$ (*) and $r_{inf}^{(2)}/R$ (**) for the $N_p=10$ case. We show in Fig. 3 B plots of $r_{inf}^{(1)}/R$, $r_{inf}^{(2)}/R$ and D/R as functions of ρ_A (Eq. (3)). It is important to note that these curves are the same, regardless of the specific parameter values of the model. We observe that all of them are decreasing functions of ρ_A or, equivalently, of N_p. N_p is a stochastic variable that changes from realization to realization. Therefore, even for a given cluster (characterized by fixed values of N, p and r_{inf}) $r_{inf}^{(1)}$ and $r_{inf}^{(2)}$ may take on different values depending on the realization. In this way, depending on r_{inf} and the values that ρ_A may take on, a subset of the events that occur at a cluster may be IP_3-binding limited (those for which $r_{inf}^{(2)}<r_{inf}$) while others are not. An analogous situation may hold regarding the Ca^{2+}-limited behavior. Furthermore, for some clusters, the Ca^{2+}-limited condition may hold for some events and the IP_3-binding limited for others. If the parameters N, p, R and r_{inf} are such that most realizations satisfy $r_{inf}^{(2)}(\rho_A)>r_{inf}$, then most events will be IP_3-binding limited. This happens if r_{inf} or pN are large enough, in which case the distribution of event sizes, P_n, approaches the distribution of available channels, P_A.

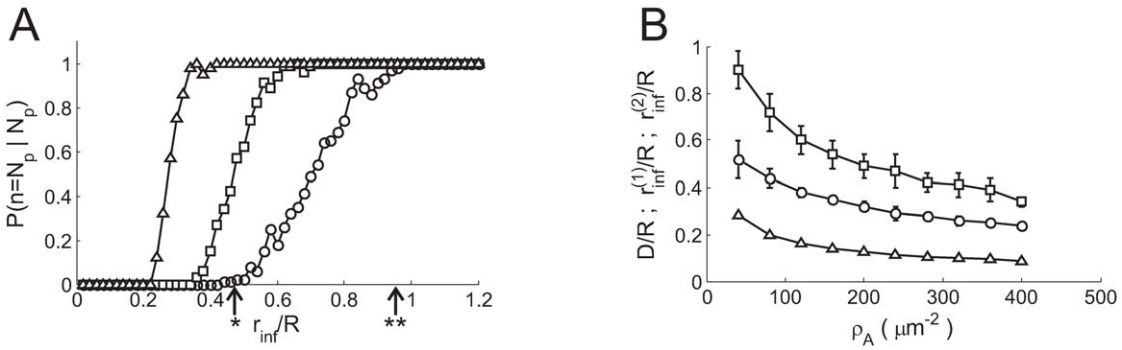

Figure 3. Percolation transition: when all available channels open during a puff. A: Probability that all available IP_3R's become open, $P(n=N_p/Np)$, as a function of the dimensionless radius of influence, r_{inf}/R, for $N_p=10$ (circles), $N_p=30$ (squares) and $N_p=100$ (triangles). B: $r_{inf}^{(1)}/R$ (circles), $r_{inf}^{(2)}/R$ (squares) and D/R (triangles) as functions of $\rho_A(N_p)=N_p/\pi R^2$. The values of $r_{inf}^{(1)}/R$ and $r_{inf}^{(2)}/R$ for the case with $N_p=10$ are indicated in A with one and two asterisks, respectively.
doi:10.1371/journal.pone.0008997.g003

Observing Percolation as a Function of Event Size

The results of Fig. 3 B imply that there are clusters that can display different types of behaviors depending on the event. For these clusters, we expect to find, in their distribution, P_n, a trace of the transition to the limiting behavior that they can display. Here we are interested in the percolation transition, *i.e.*, the transition to the IP_3-binding dominated stochasticity. As already discussed, the larger N_p the more likely it is that all IP_3R's become open during the puff (see Fig. 3 A). Thus, the transition to the IP_3-binding dominated stochasticity should occur as N_p and, consequently, n become larger. To study this transition we consider a cluster with fixed parameters R, r_{inf}, p and N (or $\lambda=pN$ in the Poisson limit) and define n^* as the minimum value of N_p such that $r_{inf}\geq r_{inf}^{(2)}(N_p)$. The definition of $r_{inf}^{(2)}$ is based on the conditional probability, $P(n=N_p/N_p)$, which is independent of N. In cases with finite N, n^* is meaningful provided that it be smaller than N. Since $r_{inf}^{(2)}$ decreases with N_p (see Fig. 3 B), taking into account the definitions of n^* and of $r_{inf}^{(2)}(N_p)$ (see Methods) we conclude that $r_{inf}>r_{inf}^{(2)}(N_p)$ and $P_o(n=N_p/N_p)\geq 0.9$ for all $N_p\geq n^*$. Thus, we can approximate:

$$P_o(n/N_p)\approx\delta_{nN_p},\qquad for\ N_p\geq n^*, \tag{4}$$

with less than 10% error. Inserting this approximation in Eq. (1) we obtain:

$$P_n=\sum_{N_p=n}^{n^*-1}P_o(n/N_p)P_A(N_p)+P_A(n),\qquad \text{if } n<n^* \tag{5}$$

$$P_n=P_A(n),\qquad \text{if } n\geq n^*. \tag{6}$$

We then conclude that the $n\geq n^*$ tail of P_n corresponds to IP_3-binding dominated events. Therefore, it should be possible to approximate it by a (renormalized) binomial (provided that $n^*\leq N$) or Poisson distribution in the region of large n. The left border of this IP_3 dominated behavior, n^*, gives information on r_{inf}, *i.e.* on the maximum distance for which CICR-coupling can work effectively. Therefore, it should be possible to estimate r_{inf} by analyzing P_n, *i.e.*, to infer a biophysical parameter that characterizes the intra-cluster dynamics from statistical information on the emergent collective behavior of the channels of the cluster.

Determining Intra-Cluster Properties from Observations of the Cluster as a Whole

We now discuss how we can estimate r_{inf} from an experimental distribution of event sizes, P_n. For the sake of simplicity, we assume that $P_A(n)$ can be approximated by a renormalized Poisson distribution, $P_\lambda(n)\equiv\lambda^n\exp(-\lambda)/((1-\exp(-\lambda))n!)$, of unknown parameter λ. The goal of this section is to provide a way to estimate λ and n^*, the value of n at which P_n and $P_A(n)\approx P_\lambda(n)$ depart from one another (see Eq. (6)). Once n^* is inferred, we estimate r_{inf}/R as $r_{inf}/R\approx r_{inf}^{(2)}(n^*)/R$ using the function displayed in Fig. 3 B. To this end, we focus on the large n tails of P_n and P_λ by computing the complementary cumulative distribution functions:

$$T_o(\ell)=\sum_{n\geq\ell}P_n, \tag{7}$$

$$T_\lambda(\ell)=\sum_{n\geq\ell}P_\lambda(n), \tag{8}$$

for $\ell\geq 2$. Given that P_λ is proportional to a Poisson distribution, there is an analytic expression for T_λ. Namely, $T_\lambda(\ell)=1-\Gamma([\ell],\lambda)/((1-\exp(-\lambda))([\ell]-1)!)$, where $\Gamma(x,y)$ is the incomplete Γ function and $[\ell]$ is the integer part of ℓ. If the cluster is such that n^* exists so that r_{inf} is larger than $r_{inf}^{(2)}(N_p)$ for $N_p\geq n^*$ and it is smaller otherwise, then, according to the calculation of the previous section, $P_n\approx P_A(n)\approx P_\lambda(n)$ for $n\geq n^*$. Therefore, the complementary cumulative distribution functions of Eqs. (7)–(8) also satisfy $T_o(\ell)\approx T_\lambda(\ell)$ for $\ell\geq n^*$.

We now describe how to estimate n^* and λ. The aim is to obtain a (renormalized) Poisson distribution, P_λ that can approximate P_n in the large n region. If we find it, we assume that it is a good approximation of the distribution of available channels, P_A. As illustrated in Fig. 1, the mean value, $\langle n\rangle_{obs}$ that is obtained using the experimental distribution, P_n, is smaller than the one that would be obtained if $P_A(n)$ was used instead. On the other hand, if P_A is a good approximation of P_n in the large n region, then the mean value obtained with P_A should be smaller than the size of the largest observed event, n_{max}. This implies that

$$\langle n\rangle_{obs}\leq\frac{\lambda}{1-\exp-\lambda}\leq n_{max}, \tag{9}$$

if P_A can be approximated by a renormalized Poisson distribution of parameter λ. Therefore, we look for the best P_λ within a finite set of renormalized Poisson distributions of parameters λ_i satisfying (9). In order to estimate r_{inf} from the observations the relevant quantity that we need to obtain is n^*, which is an integer. For this purpose, it is possible to use a rather coarse grid of λ values within the interval defined in (9). In particular, we have mainly used integer values of λ obtaining good results. Once the values λ_i are chosen, we compute the complementary cumulative distribution functions, $T_{\lambda_i}(k)$ given by (8) for each λ_i and $1 \le k \le n_{max}$. We then calculate the error of approximating $T_o(k)$ by $T_{\lambda_i}(k)$ over the interval $\ell \le k \le n_{max}$ as a function of ℓ:

$$\text{error}(T_o, T_{\lambda_i}) \equiv \frac{1}{n_{max} - \ell + 1} \sum_{k \ge \ell}^{n_{max}} |T_o(k) - T_{\lambda_i}(k)|^2. \qquad (10)$$

We set a threshold for the error, ε, and choose n_i^* for each λ_i as the smallest value of ℓ for which $error(T_o, T_{\lambda_i}) \le \varepsilon$. Finally, we choose the best λ_i as the one with the smallest n^*.

The procedure is illustrated in Fig. 4 where the "experimental" distribution comes from a simulation of our model with $R = 250nm$, $p = 5/18$, $r_{inf} = 230nm$ and $N = 18$. In this case, $n_{max} = 10$. We show in Fig. 4 A the complementary cumulative distribution functions and in Fig. 4 B the errors for the values of λ that we have considered: $\lambda_1 = 3$ (inverted triangles), $\lambda_2 = 4$ (triangles), $\lambda_3 = 5$ (squares) and $\lambda_4 = 6$ (rhombes). Larger values of λ give very bad approximations and are not shown. We show in Fig. 4 C the values, n^*, obtained for each λ using the threshold, $\varepsilon = 0.005$ (shown with a horizontal line in Fig. 4 B). In this example, the best value is $\lambda = 4$ for which $n^* = 8$. We estimate the density of IP_3-bound IP_3R's at which the departure between the experimental and the Poisson distribution occurs as $\rho_A^* = n^*/(\pi R^2) \approx 41 \mu m^{-2}$, where we have used $R = 250nm$. Using the $r_{inf}^{(2)}/R$ *vs* ρ_A relationship displayed in Fig. 3 B, we estimate $r_{inf}^{(2)}(\rho_A^*)/R \approx 0.9 \pm 0.08$ from which we get $r_{inf}^{(2)}(\rho_A^*) \approx 220nm \pm 20nm$. This provides an estimate of the radius of influence which compares very well with the value that was used to generate the data, $r_{inf} = 230nm$. Using the same procedure, we analyzed the data presented in Fig. 4D of [1] and obtained $r_{inf} = 220nm \pm 20nm$ assuming $R = 250nm$.

Discussion

Intracellular Ca^{2+} signals are built from localized release events in which Ca^{2+} enters the cytosol through one or several channels. Ca^{2+} release from the endoplasmic reticulum through IP_3R's is a key component of the Ca^{2+} signaling toolkit in many cell types. IP_3R's are Ca^{2+} channels that need to bind IP_3 and Ca^{2+} to become open and are usually organized in clusters on the membrane of the endoplasmic reticulum. The intra-cluster organization and the interactions of the channels within it affect the dynamics and extent of the signals. Therefore, their study is a matter of active research.

Recent experiments [1] that use super-resolution optical techniques are providing detailed data on elementary IP_3R-mediated Ca^{2+} release events in mammalian cells. In the experiments, the number of IP_3R- Ca^{2+}-channels that open during each event can be inferred from the observed puff amplitudes without much processing. The observations of [1] showed that the variability among clusters affected the shape of the event size distribution, P_n. In order to get rid of this variability, the distribution coming from sites with similar properties was computed in [1]. The distribution, P_n, obtained in this way was not Poisson, as we might have expected if the number of channels that opened during each event was proportional to the number of IP_3R's with IP_3 bound in the cluster [8]. The authors of [1] could reproduce P_n approximately (for events larger than a certain size) assuming a weak cooperativity among channels. Namely, they assumed that the probability that a channel became open scaled as some power of the number of open channels and obtained that the exponent was 1/3 from a fit to the data. The rationale for the cooperativity assumption relied on the fact that the IP_3R's of a cluster may be coupled via CICR induced by the Ca^{2+} ions that travel from an open IP_3R to a neighboring one. The model of [1], however, did not take space into account and did not provide a mechanistic explanation for the obtained scaling.

In this paper we have presented a simple model that includes a description of the intra-cluster spatial organization with which we can reproduce the observed distribution over all event sizes. In the model the distribution, P_n, is the result of the competition of two stochastic processes: IP_3 binding and distance-dependent CICR. The model assumes a stationarity condition, namely, that the agonists concentration at the release site is the same immediately before the occurrence of each puff. This condition holds as long as

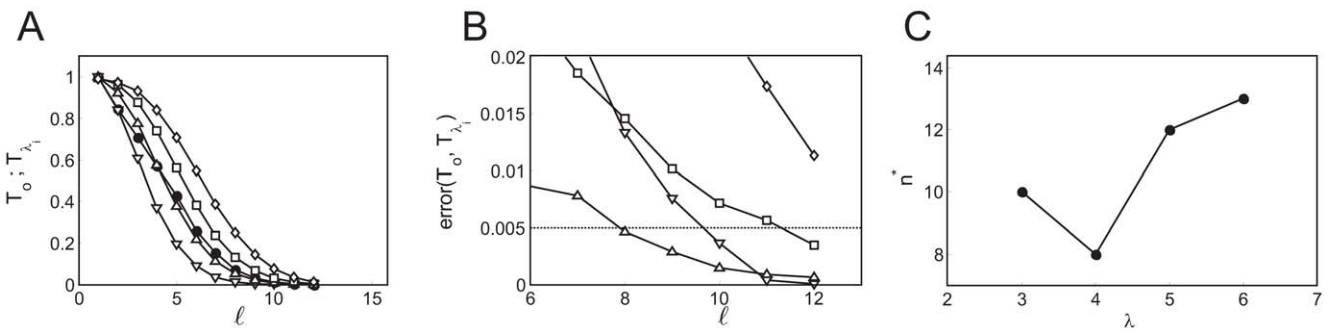

Figure 4. Change of behavior with event size. A: $T_o(\ell)$ for data obtained with our model using $R = 250nm$, $p = 5/18$, $r_{inf} = 230nm$ and $N = 18$ (solid circles). Complementary cumulative Poisson distributions, $T_{\lambda_i}(\ell)$, for $\lambda_1 = 3$ (inverted triangles), $\lambda_2 = 4$ (triangles), $\lambda_3 = 5$ (squares), $\lambda_4 = 6$ (rhombes). B: Error of approximating $T_o(k)$ by the various $T_{\lambda_i}(k)$ for $k \ge \ell$ (see text for definition) as a function of ℓ. Symbols are the same as in A. From this figure we choose $\lambda = 4$ as the one that provides the best fit to the tail of T_o. The error in the $\lambda = 6$ case is larger than 0.02 in most cases and falls outside the region displayed in the figure. C: $n^*(\lambda)$ for the four values of λ that we tested. We see that $n^*(\lambda = 4) = 8$.
doi:10.1371/journal.pone.0008997.g004

puffs are independent of one another. This is consistent with the observations reported in [1] where cluster coupling was prevented using the slow Ca^{2+} buffer EGTA and where IP_3R- Ca^{2+}-inhibition does not play a significant role. In any case, our model is adequate to describe the distribution of first event sizes that occur at each cluster before Ca^{2+} can exert any inhibiting effect.

There are two limiting cases in which one of the two stochastic processes considered in the model is the main determinant of the distribution shape. If the mean distance between IP_3R's with IP_3 bound in the cluster is much smaller than the typical distance of inter-channel coupling due to CICR for most events, the distribution is IP_3-binding limited and it can be approximated by a binomial or Poisson distribution. In the opposite case, CICR dominates and the distribution is peaked around $n \approx 1$. The Ca^{2+}-limited and the IP_3-binding limited situations can be thought of as two phases and the transition between them as a percolation-like transition in the limit in which the number of IP_3R's with IP_3 bound, N_p, is very large. This interpretation of the factors that shape the observed distribution can be tested with simulations of some of the stochastic models of intracellular Ca^{2+} signals reported in the literature (see *e.g.* [33] and references therein). They can also be tested experimentally. One possibility is to change the most likely values of N_p by changing the amount of IP_3 that is photo-released in the cell. An alternative option is to analyze P_n for events coming from clusters that give rise, on average, to larger events. According to the model, the distribution should approach a binomial or Poisson distribution as the mean value of N_p becomes larger while other parameters remain the same. Another way to affect the balance between both stochastic components is to disrupt Ca^{2+}-mediated inter-channel coupling by means of a fast buffer such as BAPTA.

Given that N_p is a stochastic variable that varies from event to event, the transition between the Ca^{2+}-dominated and IP_3-binding dominated stochasticity described by the model may be reflected in the way that P_n depends on the event size, n. In fact, we have used this property to show how a fingerprint of this transition may be encountered in P_n and how information on the inter-channel coupling distance may be extracted from it. This means that a parameter that characterizes the communication between pairs of channels can be estimated from statistical information on the emergent collective behavior of the channels of the cluster. This information could be used to analyze the effect of buffers on the intra-cluster dynamics, a matter that is of active current research [19,34]. Our model provides a simple tool with which this effect can be analyzed in experiments.

Methods

Each term of the sum that defines Eq. (1) is the product of two functions. We have an analytic expression for one of them, $P_A(N_p)$, but not for $P_o(n/N_p)$. Thus, we compute P_n numerically performing realizations of the model with fixed values of N, p, R and r_{inf}. The location of the channels within the cluster and which of them have IP_3 bound vary among realizations and are chosen randomly (see Results). We only keep realizations with $N_p \geq 1$. Once we have the spatial distribution of available IP_3R's, we start each event by picking at random one of the IP_3R's with IP_3 bound and assume it is open. If $N_p = 1$, we assume it gives rise to an event with $n = 1$. By changing the values of N, p, R and r_{inf} we analyze how P_n varies with them. In this way we can determine the values of the parameters that best reproduce the experimental observations. r_{inf} could be measured in units of the cluster spatial extent, R, in which case we would get rid of one parameter of the problem, R. We keep it to make a connection with the experimental data. However, it is important to note that the number of independent parameters of the model is 3, for finite N and 2 in the limit in which P_A can be approximated by a Poisson distribution.

For each value, N_p, of available IP_3R's, we estimate the fraction of events such that the N_p IP_3R's become open. This fraction is one for $N_p = 1$. For $N_p > 1$, we compute the probability that all available IP_3R's become open, $P(n = N_p/N_p)$, numerically, performing 500 stochastic realizations of our model for each of which we fix the value of N_p *a priori*. Namely, we fix at the beginning the values of R, r_{inf} and N_p and then pick N_p locations at random over the circle where we assume there are available IP_3R's. From there on, the model goes on as before, generating the cascade of openings that determines n. The distribution of events with n open channels for each value of N_p gives $P(n = N_p/N_p)$. This function of N_p depends on only one independent parameter, r_{inf}/R. As expected, it is an increasing function of r_{inf}/R (see Fig. 3 A).

We define two quantities, $r_{inf}^{(2)}$ and $r_{inf}^{(1)}$, which are values of r_{inf} for which $P(n = N_p/N_p)$ is either close to 1 or to 0, respectively. We compute them as follows. We first calculate a lower bound for $r_{inf}^{(2)}$ as the minimum value of r_{inf} such that, if r_{inf} is larger than this lower bound, then $P_o(n = N_p/N_p) > 0.8$. We calculate an upper bound for $r_{inf}^{(2)}$ as the minimum value of r_{inf} for which $P(n = N_p/N_p) = 1$. Then, we compute $r_{inf}^{(2)}$ as the mean between these two bounds. We assume that the distance between the bounds is the error with which $r_{inf}^{(2)}$ can be determined. We proceed analogously in the case of $r_{inf}^{(1)}$, but in this case the lower bound is the largest value of r_{inf} for which $P(n = N_p/N_p) = 0$ and the upper bound is the maximum value of r_{inf} for which $P(n = N_p/N_p) \leq 0.2$. We compute $r_{inf}^{(1)}$ and $r_{inf}^{(2)}$ in this way using the numerical estimations of $P(n = N_p/N_p)$ for various values of r_{inf}.

Acknowledgments

We acknowledge useful discussions with Ian Parker and Ian Smith and that they provide us with their experimental data. We also acknowledge Giorgio Rispoli and the other two referees for their careful reading of the manuscript and useful comments and suggestions.

Author Contributions

Conceived and designed the experiments: GS SPD. Performed the experiments: GS. Analyzed the data: GS SPD. Wrote the paper: SPD.

References

1. Smith IF, Parker I (2009) Imaging the quantal substructure of single IP_3R channel activity during Ca^{2+} puffs in intact mammalian cells. Proc Natl Acad Sci (USA) 106: 6404–6409.
2. Berridge MJ, Bootman MD, Lipp P (1998) Calcium - a life and death signal. Nature 395: 645–648.
3. DeYoung G, Keizer J (1992) A single-pool inositol 1,4,5-trisphosphate-receptor-based model for agonist-stimulated oscillations in Ca^{2+} concentration. Proc Natl Acad Sci (USA) 89: 9895–9899.
4. Fraiman D, Ponce Dawson S (2004) A model of the IP_3 receptor with a luminal calcium binding site: stochastic simulations and analysis. Cell Calcium 35: 403–413.
5. Shuai J, Pearson JE, Foskett JK, Mak DOD, Parker I (2007) A kinetic model of clustered IP_3 receptors in the absence of Ca^{2+} feedback. Biophysical Journal 93: 1151–1162.
6. Yao Y, Choi J, Parker I (1995) Quantal puffs of intracellular Ca^{2+} evoked by inositol trisphosphate in xenopus oocytes. J Physiol (Lond) 482: 533–553.
7. Shuai J, Rose HJ, Parker I (2006) The number and spatial distribution of IP_3 receptors underlying calcium puffs in *xenopus* oocytes. Biophys J 91: 4033–4044.
8. Bruno L, Ventura AC, Dargan S, Ponce Dawson S (2009) Quantifying calcium fluxes underlying calcium puffs in *xenopus laevis* oocytes. Cell Calcium;In press.
9. Ur-Rahman T, Skupin A, Falcke M, Taylor CW (2009) Clustering of IP_3 receptors by IP_3 retunes their regulation by IP_3 and Ca^{2+}. Nature 458: 655–659.

10. Sun XP, Callamaras N, Marchant JS, Parker I (1998) A continuum of IP_3-mediated elementary Ca^{2+} signalling events in xenopus oocytes. J Physiol (Lond) 509: 67–80.
11. Parker I, Yao Y (1996) Ca^{2+} transients associated with openings of inositol trisphosphate-gated channels in xenopus oocytes. J Physiol 491(Pt 3): 663–8.
12. Bootman MD, Berridge MJ, Lipp P (1997) Cooking with calcium: the recipes for composing global signals from elementary events. Cell 91: 367–373.
13. Callamaras N, Marchant JS, Sun XP, Parker I (1998) Activation and co-ordination of IP_3-mediated elementary Ca^{2+} events during global Ca^{2+} signals in *xenopus oocytes*. J Physiol 509: 81–91.
14. Swillens S, Dupont G, Combettes L, Champell P (1999) From calcium blips to calcium puffs: Theoretical analysis of the requirements for interchannel communication. Proc Natl Acad Sci (USA) 96: 13750–13755.
15. Falcke M (2003) On the role of stochastic channel behavior in intracellular Ca^{2+} dynamics. Biophys J 84: 42–56.
16. Fraiman D, Pando B, Dargan S, Parker I, Ponce Dawson S (2006) Analysis of puff dynamics in oocytes: Interdependence of puff amplitude and interpuff interval. Biophys J 90: 3897–3907.
17. Allbritton N, Meyer T, Stryer L (1992) Range of messenger action of calcium ion and inositol 1,4,5-trisphosphate. Science 258: 1812–1815.
18. Falcke M (2003) Buffers and oscillations in intracellular Ca^{2+} dynamics. Biophys J 84: 28–41.
19. Zeller S, Rüdiger S, Engel H, Sneyd J, Warnecke G, et al. (2009) Modeling of the modulation by buffers of Ca^{2+} release through clusters of IP_3 receptors. Biophys J 97: 992–1002.
20. Smith IF, Wiltgen SM, Parker I (2009) Localization of puff sites adjacent to the plasma membrane: Functional and spatial characterization of Ca^{2+} signaling in SH-SY5Y cells utilizing membrane-permeant caged IP_3. Cell Calcium 45: 65–76.
21. Ponce Dawson S, Keizer J, Pearson JE (1999) Fire-diffuse-fire model of dynamics of intracellular calcium waves. Proc Natl Acad Sci (USA) 96: 6060–6063.
22. Bär M, Falcke M, Levine H, Tsimring LS (2000) Discrete stochastic modeling of calcium channel dynamics. Phys Rev Lett 84: 5664–5667.
23. Pencea CS, Hentschel HGE (2000) Excitable calcium wave propagation in the presence of localized stores. Phys Rev E 62: 8420–8426.
24. Timofeeva Y, Coombes S (2004) Directed percolation in a two-dimensional stochastic fire-diffuse-fire model. Phys Rev E 70: 062901: 1–3.
25. Schuster S, Marhl M, Höfer T (2002) Modelling of simple and complex calcium oscillations. from single-cell responses to intercellular signalling. Eur J Biochem 269: 1333–55.
26. Shuai JW, Jung P (2002) Optimal intracellular calcium signaling. Phys Rev Lett 88: 068102: 1–4.
27. Shuai JW, Jung P (2003) Optimal ion channel clustering for intracellular calcium signaling. Proc Natl Acad Sci (USA) 100: 506–510.
28. Bugrim AE, Zhabotinsky AM, Epstein IR (1997) Calcium waves in a model with a random spatially discrete distribution of Ca^{2+} release sites. Biophys J 73: 2897–2906.
29. Skupin A, Kettenmann H, Winkler U, Wartenberg M, Sauer H, et al. (2008) How does intracellular Ca^{2+} oscillate: By chance or by the clock? Biophys J 94: 2404–2411.
30. Perc M, Green AK, Dixon CJ, Marhl M (2008) Establishing the stochastic nature of intracellular calcium oscillations from experimental data. Biophys Chem 132: 33–38.
31. Perc M, Gosak M, Marhl M (2007) Periodic calcium waves in coupled cells induced by internal noise. Chem Phys Lett 437: 143–147.
32. Perc M, Gosak M, Marhl M (2006) From stochasticity to determinism in the collective dynamics of diffusively coupled cells. Chem Phys Lett 421: 106–110.
33. Falcke M (2009) Introduction to focus issue: Intracellular Ca^{2+} dynamics— a change of modeling paradigm? Chaos: An Interdisciplinary Journal of Nonlinear Science 19: 037101.
34. Shuai J, Pearson JE, Parker I (2008) Modeling Ca^{2+} feedback on a single inositol 1,4,5-triphosphate receptor and its modulation by Ca^{2+} buffers. Biophysical Journal 95: 3738–3752.